



Visualizing the interaction of *Acanthamoeba castellanii* with human retinal epithelial cells by spontaneous Raman and CARS imaging

Journal:	<i>Journal of Raman Spectroscopy</i>
Manuscript ID	JRS-17-0226.R1
Wiley - Manuscript type:	Research Article
Date Submitted by the Author:	28-Sep-2017
Complete List of Authors:	Naemat, Abida; University of Nottingham, School of Physics and Astronomy Sinjab, Faris; University of Nottingham, School of Physics and Astronomy McDonald, Alison; University of Edinburgh, Institute of BioEngineering Downes, Andrew; University of Edinburgh, Institute for Materials & Processes; Elfick, Alistair; University of Edinburgh, Institute for Materials & Processes Elsheikha, Hany; University of Nottingham, School of Veterinary Medicine and Science Notingher, Ioan; University of Nottingham, School of Physics and Astronomy
Keywords:	<i>Acanthamoeba castellanii</i> , human cells, host-pathogen interaction, Raman micro-spectroscopy, coherent anti-stokes Raman spectroscopy

SCHOLARONE™
Manuscripts

1
2
3 **Visualizing the interaction of *Acanthamoeba castellanii* with human retinal epithelial**
4 **cells by spontaneous Raman and CARS imaging**
5
6
7
8

9 Abida Naemat,^a Faris Sinjab,^a Alison McDonald,^b Andy Downes,^b Alistair Elfick,^b Hany M.
10
11
12 Elsheikha^c and Ioan Notingher^{*,a}
13
14

15
16 ^a *School of Physics and Astronomy, University of Nottingham, Nottingham, NG7 2RD, United*
17
18 *Kingdom*
19

20 ^b *School of Engineering, Institute for BioEngineering, University of Edinburgh, The King's*
21
22 *Buildings, Mayfield Road, Edinburgh EH9 3DW, United Kingdom*
23
24

25 ^c *School of Veterinary Medicine and Science, University of Nottingham, College Road,*
26
27 *Leicestershire, LE12 5RD, United Kingdom*
28
29

30
31
32
33
34 *Ioan Notingher, *E-mail:* ioan.notingher@nottingham.ac.uk; Tel: +44 0115 951 5172
35
36
37
38
39
40
41
42
43
44
45
46
47
48
49
50
51
52
53
54
55
56
57
58
59
60

Abstract

Improved understanding of the mechanism of nutrient's uptake can enable targeted manipulation of nutrient sensing pathways in medically important pathogens to a greater degree than is currently possible. In this context, we present the use of spontaneous Raman micro-spectroscopy (RMS) and coherent anti-Stokes Raman spectroscopy (CARS) to visualise the time-dependent molecular interactions between the protozoan *Acanthamoeba castellanii* and host human cells. Human retinal pigment epithelial (ARPE-19) cells were pre-labelled with deuterated Phe (L-Phe(D8)) and the uptake of the host derived L-Phe(D8) by *A. castellanii* trophozoites was measured by RMS for up to 48 hours post infection (hpi). This approach revealed a time-dependent uptake pattern of this essential amino acid by *A. castellanii* trophozoites during the first 24 hpi with complete enrichment with L-Phe(D8) detected in trophozoites at 48 hpi. In contrast, cell free *A. castellanii* trophozoites showed a modest uptake of only 16-18% L-Phe(D8) from L-Phe(D8)-supplemented culture medium after 3h, 24h and 48h hpi. CARS microscopy was successfully used to monitor the reprogramming of lipids within the trophozoites as they engaged with host cells. The methodology presented here provides new advances in the ability to analyze the kinetic of amino acid acquisition by *A. castellanii* from host cell and extracellular environment, and to visualize lipid reprogramming within the trophozoite.

Key words: *Acanthamoeba castellanii*; Coherent anti-Stokes Raman scattering; Host-pathogen interaction; Isotope labelling; Raman Spectroscopy

Introduction

Acanthamoeba species are single cell eukaryotic protozoa that can survive in a variety of environmental niches, including soil and water,¹ swimming pools,² eye wash stations,³ and noses and throats of asymptomatic individuals.⁴ *Acanthamoeba* exists in two different life cycle forms: trophozoite and cyst. Under favourable conditions, such as abundant food supply, appropriate temperature, osmolarity and neutral pH, *Acanthamoeba* exists in the vegetative, infective and replicative trophozoite stage. In this form of the life cycle, the organism has a diameter of 10-25 μm ⁵ and exhibits irregular shape with locomotor pseudopods and surface acanthopodia,⁶ Under stress, the trophozoite stage transforms into a metabolically inactive cyst⁷ and encloses itself within a thick wall and becomes resistant to biocides, chlorination and antibiotics.⁸ Cystic stage transforms back to the trophozoite form with improved conditions in a process known as excystment. Although considered as free-living ubiquitous protozoans, several species of *Acanthamoeba* can cause severe infections in humans, mainly localized in immune privileged sites, such as the brain⁸ and the eyes.⁹

Despite the considerable efforts to elucidate the pathogenesis of diseases caused by *Acanthamoeba castellanii* infection, there are still many gaps in our understanding of the mechanisms that drive the interaction between this organism and host cells. One such mechanism that significantly impacts the parasite pathogenicity is the pathways by which *A. castellanii* trophozoites access nutrients from their host cells in infected tissues. It is a known fact that *A. castellanii* trophozoites display striking differences in their metabolic functions once they become colonized by bacterial as compared to non-colonized trophozoites. For examples, increase in the concentration of free amino acids in the cytosol of *A. castellanii* was attributed to activation of the amoebal proteasome by *Legionella pneumophila* AnkB protein.¹⁰ Also, there is evidence that amino acids auxotrophy of *L. pneumophila* and its amoebic host was synchronized during evolution.¹¹

1
2
3 Recent data revealed an active shikimate pathway in *A. castellanii* and was proven
4 essential for the synthesis of aromatic amino acids.^{12,13} Mass spectrometry-based ¹³C
5 isotopologue profiling of ¹³C-prelabeled *A. castellanii* trophozoites revealed that this parasite
6 is capable of *de novo* biosynthesis of nine amino acids, namely Ala, Asp, Glu, Ser, Phe, Tyr,
7 Pro, Gly, and Thr. On the other hand, Val, Leu, Ile, Lys, and His did not acquire any ¹³C
8 label, indicating that *de novo* synthesis from glucose was not detectable for these five amino
9 acids. However, there appears to be no or little work experimentally testing this relationship
10 in the context of *A. castellanii* interaction with mammalian host cells. Indeed, our
11 understanding of this crucial process is still limited because of various experimental and
12 conceptual challenges.
13
14
15
16
17
18
19
20
21
22
23
24

25 Spontaneous Raman micro-spectroscopy (RMS) provides detailed molecular analysis of
26 individual cells with micrometric spatial resolution.¹⁴⁻¹⁸ With the exception of *Plasmodium*
27 *falciparum*,¹⁹⁻²¹ reports of RMS studies of protozoan parasites have been limited. Selective
28 scanning RMS imaging was used to detect *Neospora caninum* tachyzoites colonizing human
29 brain microvascular-endothelial cells.²² RMS time-course studies over 48 hours were used to
30 determine the molecular changes in the apicomplexan protozoan parasite *Toxoplasma gondii*
31 and in their surrogate human retinal pigment epithelial (ARPE-19) cells.²³ More recently,
32 stable isotope labelling of the aromatic amino acid phenylalanine (Phe) combined with RMS
33 enabled real-time monitoring of the molecular exchange of Phe between *T. gondii* engaging
34 with ARPE-19 cells, non-invasively.²⁴ RMS has also been used with isotope labelling
35 technology to differentiate the cellular components produced through distinct metabolic
36 pathways,²⁵⁻²⁸ lipid uptake and metabolism inside human macrophages on a single cell level
37
38
39
40
41
42
43
44
45
46
47
48
49
50
51
52
53
54
55
56
57
58
59
60

1
2
3 *Acanthamoeba* in ocular infections following exposure to polyhexamethylene biguanide
4 (PHMB), a polymer used as a disinfectant and antiseptic for the treatment of *Acanthamoeba*
5 keratitis.³²
6
7

8
9
10 Coherent anti-Stokes Raman scattering (CARS) microscopy is a complementary and
11 closely related technique to spontaneous Raman spectroscopy which allows fast high-
12 resolution 3D imaging of cells.³³⁻³⁵ CARS has been successfully used for various
13 applications in the life sciences, particularly in lipid biology, from imaging lipid
14 membranes³³, to endogenous cellular lipid droplet distributions^{33,36} and even whole-organism
15 lipid imaging.³⁷ The use of two excitation lasers with a frequency difference tuned to a
16 particular vibrational band amplifies the Raman response by a nonlinear optical interaction,
17 allowing much faster measurement of a sample at a single Raman band. The most common
18 Raman band used to generate image contrast with CARS is the CH₂ symmetric stretching
19 band at ~2845cm⁻¹, which is a reliable lipid biomarker.
20
21
22
23
24
25
26
27
28
29
30

31
32 In the present study, we utilized RMS-coupled with isotope labelling and CARS imaging
33 to characterize the uptake of amino acid Phe by *A. castellanii* trophozoites from human
34 ARPE-19 cells. Because the frequencies of the vibrational modes of Phe depend on the mass
35 of the atoms, the substitution of hydrogen with deuterium decreases the wavenumber of the
36 characteristic Raman bands. This makes it possible to discriminate between Phe molecules
37 originating from the human cells and *Acanthamoeba*. With the use of high-resolution CARS,
38 we also investigated whether the interaction of *A. castellanii* trophozoites with host cells
39 triggers reprogramming of lipid contents within trophozoites.
40
41
42
43
44
45
46
47
48
49
50

51 **Experimental**

52 **Cell culture conditions**

1
2
3 As an immune-privileged and easily accessible organ, the eye constitutes a favorable target
4 for *A. castellanii*. Therefore, human retinal pigment epithelial (ARPE-19; American Type
5 Culture Collection, Manassas, VA) cell line, which represents the main constituent of the
6 blood-retinal barrier was selected as a model to investigate the molecular changes that
7 accompany *A. castellanii* infection to the ocular surface. ARPE-19 cells were used at passage
8 11 and were maintained in DMEM supplemented with 1% penicillin/streptomycin and 5%
9 heat-inactivated fetal bovine serum (FBS). Cells were incubated in 5% CO₂ incubator at 37°C
10 and were passaged twice weekly. Cell viability was determined by trypan blue exclusion
11 assay and cells were used in the experiments when their viability is >98%.
12
13
14
15
16
17
18
19
20
21
22

23 24 25 **Parasite strain and growth conditions**

26
27 *Acanthamoeba castellanii* T4 genotype, originally obtained from the American Type Culture
28 Collection (ATCC #50492), was used in the study. *Acanthamoeba castellanii* trophozoites
29 were grown in T-75cm² tissue culture flasks (Sarstedt, UK) in autoclaved axenic peptone-
30 yeast-glucose (PYG) medium comprising 0.75% w/v proteose peptone (Oxoid™, Thermo-
31 Fisher Scientific, UK), 0.75% w/v yeast extract, and 1.5% w/v glucose in distilled water.
32 Flasks were maintained in a humidified standard air incubator at 25°C. Every 3-5 days the
33 growth PYG medium was removed from culture flasks and replaced with fresh medium.
34 Under these conditions more than 90% of *A. castellanii* remained bound to the flask as
35 trophozoites.
36
37
38
39
40
41
42
43
44
45
46
47
48

49 **Stable Isotope Labelling by Amino Acids (SILAC)**

50
51
52
53
54 The aim of this experiment was to determine the molecular exchange between host ARPE-19
55 cells and *A. castellanii* trophozoites. The ARPE-19 cells were cultured in a specially-
56
57
58
59
60

1
2
3 formulated medium containing all amino acids in unlabelled form, but Phe, which was added
4
5 with the desired isotope label. To minimize the background signal of the L-Phe, ARPE-19
6
7 cells were synchronized overnight in serum-deficient, Phe-free customized DMEM culture
8
9 medium. The cells were subsequently incubated with SILAC DMEM medium supplemented
10
11 with L-Phe(D8). The doubling time (DT) of ARPE-19 cells grown *in vitro* was determined
12
13 daily for a period of 6 days via cell counting using automated cell counter (LUNA-II™,
14
15 Labtech International Ltd., East Sussex, UK). After complete substitution of L-Phe by L-
16
17 Phe(D8) in ARPE-19 cells (defined as $I_{960}/(I_{960}+I_{1004})=1$, where I_{960} and I_{1004} are the
18
19 intensities of Raman bands at 960 cm^{-1} and 1004 cm^{-1}), the cells are challenged with *A.*
20
21 *castellanii* trophozoites as described below.
22
23
24
25
26
27

28 **Infection of host cells with *A. castellanii***

29
30 ARPE-19 cells (10^4 cells/ml) labelled with L-Phe(D8) were seeded in titanium cell-chambers
31
32 (sample holders), which were fitted in 6-well plastic cell culture plates, with a volume of 2 ml
33
34 DMEM/chamber. The sample holders were purpose-built to enable acquisition of Raman
35
36 spectra of the cells and incorporated MgF2 coverslips (0.17 mm thick) at the bottom. Before
37
38 introducing the parasites to ARPE-19 cells the culture medium was replaced with L-Phe-free
39
40 media to avoid any false labelling of the parasite. Parasites were grown in PYG medium, but
41
42 they were transferred to L-Phe-free DMEM media during host cell infection. The only source
43
44 of L-Phe(D8) to the parasites came from the labelled host cells and L-Phe for host cells was
45
46 from the parasites. Infection was initiated by adding *A. castellanii* trophozoites at a
47
48 multiplicity of infection of 1 cell to 1 parasite. During Raman spectral mapping of live cells,
49
50 *A. castellanii* trophozoites were found to move beyond the designated area of imaging before
51
52 the completion of raster scan measurement at 0.5 seconds acquisition time. Thus, we had to
53
54
55
56
57
58
59
60

1
2
3 perform the measurements on trophozoites fixed with 4% paraformaldehyde before starting
4
5 the Raman spectral imaging.
6
7
8

9 10 **L-Ph(D8) uptake by isolated *A. castellanii* trophozoites**

11 We were also interested in testing the ability of isolated trophozoites to acquire L-Phe(D8)
12 from the culture medium. To achieve this, we harvested 2×10^7 *A. castellanii* trophozoites
13 from cultured flasks, followed by washing in 10 ml of sterile Dulbecco's phosphate-buffered
14 saline three times to remove any traces of PYG medium. The trophozoite pellet was then
15 suspended in 2 ml of L-Ph(D8)-supplemented medium and were subjected to Raman imaging
16 for 24 hours.
17
18
19
20
21
22
23
24
25

26 27 **Spontaneous Raman micro-spectroscopy (RMS)**

28 Raman spectra were recorded using a purpose-built confocal Raman micro-spectrometer
29 optimized for studying cell biology and host-parasite interaction. An inverted microscope
30 (IX71, Olympus, Essex, UK) was used for the setup because it allows cell measurements
31 without the limitation of the objective lens dipping in and contaminating the culture media as
32 opposed to up-right microscopes. The laser is focused through a MgF2 coverslip at the
33 bottom of specially designed sample holders. A 785 nm ~ 170 mW laser (before objective)
34 (Ti:sapphire laser, spectra-physics) was used for excitation of Raman spectra. To maximize
35 the spatial resolution and collection efficiency for the Raman spectra, a 60×/1.20 NA water-
36 immersion objective (Olympus) was used to focus the laser (beam diameter expanded to
37 match the objective pupil, laser spot ~700 nm on sample) on individual cells as well as for
38 collection of Raman scattered photons. The Raman scattered light was collimated and then
39 focused on a 50-mm diameter optical fiber connected to a spectrometer equipped with a 830
40 lines per mm grating (spectral resolution of 1.5 cm^{-1} in the 600–1800 cm^{-1} region) and cooled
41
42
43
44
45
46
47
48
49
50
51
52
53
54
55
56
57
58
59
60

1
2
3 deep-depletion back-illuminated CCD detector (Andor Technologies, Belfast, UK). Raman
4
5 spectral imaging was performed by scanning areas of the trophozoites through the laser focus
6
7 in a raster pattern (1 μm step size) using a high-precision step-motor stage (Prior, Cambridge,
8
9 UK) and acquiring Raman spectra at each position (1s per pixel). The spectrometer
10
11 wavenumber axis was calibrated prior to each experiment using tylenol at an accuracy of 0.5
12
13 cm^{-1} .
14
15

16 17 18 **CARS microscopy**

19
20
21
22
23 CARS images were acquired using a custom built multi-modal multiphoton microscope as
24
25 described in Moura et al ³⁸. This system consists of a mode-locked ND:YVO4 laser source
26
27 (PicoTrain, Spectra Physics) to generate the Stokes pulse (6ps, 1064 nm) and also a 532nm
28
29 output which is coupled into an optical parametric oscillator (OPO) providing tuneable
30
31 excitation across 700-1000nm (Levante Emerald, APE). The two beams are coupled into an
32
33 inverted microscope (Eclipse TE2000U, Nikon) with a Nikon BV 'C1' scanhead. Both beams
34
35 were overlapped spatially and temporally on to the sample using a 25 \times /1.05 NA water-
36
37 immersion objective lens (Olympus). The CARS signal was acquired at the 2845 cm^{-1} Raman
38
39 resonance by tuning the OPO to 817 nm wavelength. All images were acquired with 115 mW
40
41 (817 nm) and 80mW (1064 nm) of excitation power at the sample plane.
42
43
44

45 46 **Fluorescence Staining**

47
48 Acridine orange (AO) staining was used to differentiate the morphological features of *A.*
49
50 *castellanii* trophozoites from the host ARPE-19 cells. As a DNA intercalating dye, AO is
51
52 used to differentially stain RNA and DNA inside eukaryotic cells. ARPE-19 Cells were fixed
53
54 in 4% paraformaldehyde for 15 min, followed by washing with 1x phosphate buffered saline
55
56 (PBS) twice. Fixed cells were incubated with 5% AO staining solution for 10 min. Imaging
57
58
59
60

1
2
3 of AO-stained *A. castellanii*-infected ARPE-19 cells was performed, on the same cell, after
4 completion of the Raman spectral imaging. Imaging was performed by using wide-field
5 fluorescent microscope integrated on the confocal Raman micro-spectrometer. The
6 retrospective positioning and identification of the cells was based on two thin marks engraved
7 on the cell chambers (retro-positioning accuracy was 5 μm).
8
9
10
11
12
13
14
15

16 **Image analysis and data processing**

17
18 Data pre-processing and analysis was done by using in-house built functions in Matlab (The
19 MathWorks, Natick, MA). The process of data pre-processing involved cosmic rays removal
20 and background subtraction. The cosmic ray correction algorithm was design to detect the
21 regions of the Raman spectra that had a gradient higher than the average gradient $\pm 10 \times$ the
22 standard deviation. Once, detected, the algorithm removed 7 data points at the corresponding
23 region and replaced them with values based on a linear extrapolated for that region. The
24 background spectra were measured for each sample, and represented the mean of 100 Raman
25 spectra measured as a 10 $\mu\text{m} \times 10 \mu\text{m}$ raster scan in areas close to the cells of interest. Noise
26 in the resulting data matrix was reduced by using singular value decomposition. The spectral
27 images presented in Figures 1-6 were obtained by calculating the height of the specified
28 Raman bands after subtraction of a local linear baseline for each particular band.
29
30
31
32
33
34
35
36
37
38
39
40
41
42
43
44

45 **Results**

46 **Uptake of L-Phe(D8) by *A. castellanii* from SILAC Media**

47
48 As a baseline, we first investigated whether *A. castellanii* can acquire L-Phe(D8) from the
49 culture medium in the absence of host human cells. For this purpose, *A. castellanii*
50 trophozoites were grown in normal medium conditions containing L-Phe and were
51
52
53
54
55
56
57
58
59
60

1
2
3 subsequently incubated in media supplemented with L-Phe(D8). After 24 hours of incubation
4
5 in the L-Phe(D8)-supplemented medium, Raman spectral imaging was performed. Raman
6
7 bands were selected to map the distribution of lipids and proteins (1449 cm^{-1}), nucleic acids
8
9 (786 cm^{-1}), L-Phe (1004 cm^{-1}), and L-Phe(D8) (960 cm^{-1}), as shown (Fig. 1). The results
10
11 show that Raman spectra of *A. castellanii* consist of bands typically assigned to lipids,
12
13 proteins and nucleic acids, similar to other cell types.^{14,15} The most intense bands can be
14
15 assigned to molecular vibrations of lipid molecules, such as the C=C stretching 1660 cm^{-1} ,
16
17 CH₂ deformation 1449 cm^{-1} , CH₂ twisting 1303 cm^{-1} , =C-H deformations 1260 cm^{-1} ,
18
19 symmetric stretching of N(CH₃)₃ of choline group 719 cm^{-1} . Raman bands corresponding to
20
21 vibrational modes of the sugar-phosphate backbone in nucleic acids were identified at 788
22
23 cm^{-1} (O-P-O bonds) and 1098 cm^{-1} (PO₂⁻). The most intense Raman bands characteristic to
24
25 proteins were observed at $\sim 1660\text{ cm}^{-1}$ and $1300\text{-}1400\text{ cm}^{-1}$, and were assigned to the Amide I
26
27 and Amide III vibrations. CH₂ vibrations of protein molecules also contributed to the 1445
28
29 cm^{-1} band. Of particular interest in this study is the ring-breathing mode of Phe, which was
30
31 identified at 1004 cm^{-1} in native L-Phe. The wavenumber of this band is red-shifted to 960
32
33 cm^{-1} in L-Phe(D8) molecules.^{24,28} Thus, this was used in our study to analyze the uptake of L-
34
35 Phe by *A. castellanii*.
36
37
38
39

40
41 Figure 1 shows that the nucleus of *A. castellanii* can be identified as the region
42
43 corresponding to the highest intensity in the Raman map corresponding to the 786 cm^{-1} band.
44
45 The nucleus region was also characterised by a high concentration of proteins (1004 cm^{-1} and
46
47 1449 cm^{-1} maps). Regions of high concentration of lipids was also observed at locations (iii)
48
49 and (iv) in the 1449 cm^{-1} map. At these locations, the 1303 cm^{-1} and 1660 cm^{-1} bands have
50
51 high intensity. To provide an analysis of the overall uptake of L-Phe(D8) by *A. castellanii*
52
53 from the culture medium, mean Raman spectra of individual *A. castellanii* were calculated by
54
55 averaging all Raman spectra in the raster scan covering the area of the cell. Figure 2 presents
56
57
58
59
60

1
2
3 spectral images of three typical *A. castellanii* and their mean Raman spectra. The uptake ratio
4 of L-Phe(D8) was calculated by considering the intensity (height) of the L-Phe (I_{1004}) and L-
5 Phe(D8) (I_{960}) bands by using the formula $I_{960}/(I_{1004}+I_{960})$. This analysis showed that the
6 concentration of L-Phe(D8) acquired by *A. castellanii* from the media in 24 hours represent
7 16-18% of the total amount of L-Phe in the trophozoites.
8
9

10 Uptake of L-Phe(D8) by *A. castellanii* from ARPE-19 cells

11 To investigate the exchange of L-Phe during the host-pathogen interaction, human ARPE-19
12 cells pre-labelled with L-Phe(D8) were inoculated with *A. castellanii* trophozoites. After 24
13 hpi, the interacting parasites and host cells were fixed in paraformaldehyde and measured by
14 Raman raster scanning. Figure 3 presents typical Raman spectral maps corresponding to the
15 native L-Phe (1004 cm^{-1}) and the labelled L-Phe(D8) (960 cm^{-1}), along with the maps
16 corresponding to the 1449 cm^{-1} band.
17
18

19 The presence of the 960 cm^{-1} band and absence of the 1004 cm^{-1} band in the selected
20 Raman spectra of the ARPE-19 cells indicate that human cells contain L-Phe(D8), but not L-
21 Phe. On the other hand, Figure 3 shows the presence of the 960 cm^{-1} band also in the Raman
22 spectra of *A. castellanii*, an indication of the uptake of L-Phe(D8) from the ARPE-19 cells. It
23 is also interesting to note that the Raman image corresponding to the 1449 cm^{-1} band
24 indicates a higher concentration of lipids at the junction between the *A. castellanii* and the
25 ARPE-19 cell. However, the mean Raman spectra of *A. castellanii* in Figure 4 indicate that at
26 this time point, the intensity of the 960 cm^{-1} band varied widely from cell to cell. A higher
27 intensity of the 960 cm^{-1} band was associated with a decrease in the intensity of the L-Phe
28 1004 cm^{-1} , such as in the case of samples 1 and 2 in Figure 4. The Raman spectra of some *A.*
29 *castellanii*, e.g. Sample 3, indicated a complete saturation with L-Phe(D8) at 24 hpi.
30
31

32 Figure 5 presents Raman spectral maps of ARPE-19 cells infected with *A. castellanii* at
33 48 hpi. At this time point, the 1004 cm^{-1} Raman band corresponding to the native L-Phe can
34
35
36
37
38
39
40
41
42
43
44
45
46
47
48
49
50
51
52
53
54
55
56
57
58
59
60

no longer be detected. The distribution of proteins appears homogenous (map corresponding to the 960 cm^{-1} band), while regions of high concentration of lipids can be identified at the periphery of the cell (1449 cm^{-1} map position iv). Intense bands assigned to nucleic acids (786 cm^{-1} band) can also be identified at position (iii), indicating the location of the nucleus.

The mean Raman spectra (Fig. 6) of *A. castellanii* trophozoites at 48 hpi indicate that bands assigned to Phe were detected only at 960 cm^{-1} . This result indicates that for all *A. castellanii* at 48 hpi, the native L-Phe was completely substituted with L-Phe(D8) uptaken from the host ARPE-19 cell.

Dynamic of uptake of L-Phe(D8) at single parasite level

The uptake of Phe by *A. castellanii* from the ARPE-19 host cells was expressed as the percentage of L-Phe(D8) from the total Phe, and was calculated as the ratio $I_{960}/(I_{960}+I_{1004})$. Figure 7a shows that compared to *A. castellanii* grown in L-Phe(D) media, for which $I_{960}/(I_{960}+I_{1004})=0.2$ at 24 hours, the 50% of the L-Phe in *A. castellanii* infecting ARPE-19 cells has been acquired from the human cells as L-Phe(D8) ($I_{960}/(I_{960}+I_{1004})=0.5$). Nevertheless, the ratio showed large variations among cells (as also shown in Fig. 3), which is reflected in the large error bars in Fig. 7. At 48 hpi, complete substitution of L-Phe with L-Phe(D8) was typically observed in all *A. castellanii* ($I_{960}/(I_{960}+I_{1004})=1$).

The difference between the Raman spectra of *A. castellanii* infecting ARPE-19 cells and spectra of *A. castellanii* in medium containing L-Phe(D8) were calculated in order to investigate any changes related to L-Phe metabolism. In particular, we focused on whether L-Phe(D8) was involved in the metabolism of tyrosine, by analyzing the 854 cm^{-1} and 834 cm^{-1} Fermi resonance doublet. This resonance is due to the interaction between the ring-breathing fundamental (ν_1) and the overtone of the nonplanar ring vibrations (ν_{16a}).³⁶ In the case of liquid p-cresol (doublet 842 cm^{-1} and 824 cm^{-1} , ν_{16a} at 413 cm^{-1}), the substitution of H with D

atoms removed the resonance because of the downshift of both vibrational modes, and typically only the ν_1 band was observed in the Raman spectra: 824 cm^{-1} for p-cresol-2,6-D₂ (ν_{16a} at 386 cm^{-1}) and 791 cm^{-1} for p-cresol-D₄ (ν_{16a} at 362 cm^{-1}).³³ Based on these arguments, the presence of any deuterated tyrosine molecules following a potential metabolism of L-Phe(D₈) by *A. castellanii* should make only the ν_1 band detectable in the Raman spectra as a consequence of the removal of the Fermi resonance. In addition, the ν_1 band is expected to downshift to the $854\text{--}790\text{ cm}^{-1}$ region. Nevertheless, the results in the difference spectra corresponding to *A. castellanii* and 48 hpi (Fig. 7b) indicate an increase in the 854 cm^{-1} band assigned to ν_1 , but no decrease in the intensity of the 834 cm^{-1} band to support the removal of the Fermi resonance. These spectral differences are consistent with changes in the ratio of intensities of the doublet, that may be related to the state of the hydroxyl groups in tyrosine, but show no evidence of the presence of deuterated tyrosine molecules in *A. castellanii*.

In order to obtain higher resolution visualization of the infection process, we utilized coherent anti-Stokes Raman scattering (CARS) microscopy for label-free observations of lipid structures in cells at different time-points after infection. Figure 8 shows example CARS images of *A. castellanii* and ARPE-19 cells at 3h, 24h and 48h post-infection. The high-wavenumber region of the Raman spectra contained strong bands corresponding to the C-H₂ symmetric stretching at 2845 cm^{-1} . The higher number of C-H₂ bond in lipid molecules compared to other common biomolecules, makes CARS a powerful technique for lipid imaging. Images were generated from maximum intensity z-projections of 3D imaging datasets (processed in ICY software³⁹) which allows the total lipid content to be measured in the range from the coverslip surface to typically $5\text{--}20\text{ }\mu\text{m}$ above. *Acanthamoeba* trophozoites can be identified relatively easily with these 3D CARS datasets, as these cells typically do not spread out flat across the coverslip as were ARPE-19 cells. Also, the high spatial resolution

1
2
3 allowed the vacuoles and concentrated structures within the cytoplasm/nucleus to be
4
5 observed.

6
7 The CARS images also revealed some phenotypic changes at different time-points after
8
9 infection. At 24 and 48 hpi, most of the *Acanthamoeba* trophozoites were rounded in shape,
10
11 whilst several at the 3hr time-point were elongated, suggesting they were fixed as they were
12
13 migrating across the host cell surface. Also, the concentration of lipid droplets within the
14
15 trophozoites relative to the immediate surrounding appears to increase with time. The lipid
16
17 droplet distribution in ARPE-19 cells at later time-points also appeared to be less uniform,
18
19 with droplets appearing to collect close to the interface between them and any trophozoites in
20
21 close proximity. This extensive lipid reprogramming suggests a coordinated response of the
22
23 infected host cells as the trophozoites interact with them.
24
25
26
27
28
29

30 Discussion

31 We developed a methodology that combines Raman spectroscopy and stable isotope labelling
32
33 to monitor molecular changes that occur during the interaction of the extracellular parasite *A.*
34
35 *castellanii* with host ocular tissue using human ARPE-19 cells as a model. Our aim was to
36
37 interrogate the amoeba's ability to acquire L-Phe(D8) from host cells. We also monitored the
38
39 parasite's ability to uptake L-Phe(D8) while in isolation (i.e., growing freely in cell free L-
40
41 Ph(D8)-supplemented medium). CARS imaging was also used for higher resolution structural
42
43 imaging based on the Raman resonance at 2845 cm^{-1} , particularly showing the distribution of
44
45 lipid droplets within the trophozoites at different time points after infection. This combined
46
47 approach allowed us to investigate the relative importance of metabolic exchange between *A.*
48
49 *castellanii* and its host cells *in vitro* and provided information on amoeba-specific changes in
50
51 chemical composition during interaction with ARPE-19 cells.
52
53
54
55

56 It was notable that extracellular *A. castellanii* trophozoites were not capable of acquiring
57
58
59
60

1
2
3 L-Phe(D8) while growing in cell-free medium. Raman band related to isotope labelled L-
4 Phe(D8) at 960 cm^{-1} was very small even at 24 hours of incubation in L-Ph(D8)-
5 supplemented medium. On the other hand, when *A. castellanii* trophozoites were introduced
6 to ARPE-19 cells, they showed fast uptake of L-Phe(D8), which was solely sourced from the
7 host ARPE-19 cells as the medium used in the infection experiment did not contain any L-
8 Ph(D8). On average, *A. castellanii* trophozoites measured at 24 hpi showed uptake ratios
9 between 40-60% of L-Phe (D8) from host cells. These results demonstrate that the uptake
10 ratio of L-Ph(D8) is enhanced by the physical contact between the host cell and the parasite.
11 The importance of binding with host cells and protein trafficking in the initiation of *A.*
12 *castellanii* infection has been demonstrated previously, showing that adhesion and secretion
13 of a mannose-induced protein (MIP-133) by clinical *A. castellanii* isolate causes damage of
14 corneal epithelial cells and that these cytopathic effects were mitigated by using chicken
15 specific anti-MIP-133 antiserum.⁴¹

16
17
18
19
20
21
22
23
24
25
26
27
28
29
30
31
32 It is likely that parasites that are more quickly able to engage with host cells are those
33 ones that are detected with complete substitution of L-Phe(D8) at 24 hpi. At 48 hpi, all the
34 parasites were found completely enriched with L-Phe(D8). The clinical *A. castellanii* strain
35 used in the present study is of the T4 genotype, which is known to bind more firmly to host
36 target cells and leads to more cytotoxicity than other *A. castellanii* genotypes,⁴² which may
37 explain the significant link between the T4 genotype with human corneal disease. These
38 findings agree and contrast with results obtained in the apicomplexan protozoan parasite
39 *Toxoplasma gondii*. While host cell free *A. castellanii* and *T. gondii* were less competent in
40 acquiring L-Phe(D8) from culture medium, *T. gondii* tachyzoites were able to acquire L-
41 Phe(D8) from host cells very efficiently with uptake rates estimated as high as 10^4
42 molecules/second.²²

1
2
3 These findings reveal significant differences of amino acid uptake kinetics between these
4 two different parasites, reflecting perhaps their different lifestyles. *T. gondii* is a strictly
5 intracellular pathogen and has coevolved with its hosts in order to efficiently infect, replicate
6 within, and be transmitted to new hosts to ensure survival and a continual infection cycle.
7 Hence, dependence on host cells is fundamental for the survival of this pathogen. In contrast,
8
9
10
11
12
13
14 *A. castellanii* is predominantly a free-living amoeba and causes disease under certain
15 circumstances. Also, because amoeba organisms live under harsh conditions they developed a
16 remarkable ability to adapt to numerous environmental factors (e.g., forming cysts)⁷ and to
17 become less reliant on host to survive. Recent isotopologue profiling analysis showed that *A.*
18 *castellanii* can synthesize *de novo* nine amino acids, namely Ala, Ser, Glu, Asp, Pro, Gly,
19 Phe, Tyr, and Thr, whose precursors stem from degradation products of glucose via
20 glycolysis, the PPP, and the TCA pathway, respectively. In contrast, the parasite cannot
21 synthesize five AAs (Ile, Leu, Val, His, and Lys),¹² indicating that the amoeba is auxotrophic
22 for these amino acids. Earlier studies showed that *Acanthamoeba* minimal medium requires
23 to be supplemented with Ile, Leu, Val, Arg, and Met, as long as glucose is present as a single
24 carbon source,⁴³ but Gly is needed for growth in minimal medium if acetate is the sole carbon
25 source. Also, acetate was not found to be a suitable carbon/energy source for another
26 *Acanthamoeba* species, *A. culbertsoni*.⁴⁴ Our results are interesting because despite the ability
27 of *A. castellanii* trophozoites to synthesize aromatic amino acids *de novo*¹² as they possess
28 genes for the shikimate pathway,⁴⁵ *A. castellanii* still acquires Phe efficiently from host cells.

29
30
31
32
33
34
35
36
37
38
39
40
41
42
43
44
45
46
47
48
49
50
51
52
53
54
55
56
57
58
59
60

Acanthamoeba trophozoites appeared to have a higher lipid concentration at 24 and 48 hpi relative to the surrounding areas than at 3 hours, suggesting a subversion of host lipids. *Acanthamoeba* is rich in lipids; its plasma membrane consists of phospholipids (25%), sterols (13%), lipophosphoglycan (29%), and proteins (33%).^{46, 47} Phosphatidylcholine (45%), phosphatidylethanolamine (33%), phosphatidylserine (10%), phosphoinositide (6%), and

1
2
3
4
5
6
7
8
9
10
11
12
13
14
15
16
17
18
19
20
21
22
23
24
25
26
27
28
29
30
31
32
33
34
35
36
37
38
39
40
41
42
43
44
45
46
47
48
49
50
51
52
53
54
55
56
57
58
59
60

diphosphatidylglycerol (4%) constitute the major phospholipids in *Acanthamoeba*. The main fatty acids chains in this organism are oleic acids (40-50%), and longer polyunsaturated fatty acids (20-30%).⁴⁸ *Acanthamoeba* also contains low levels of glycolipids and glucose accounts for about 60% of the sugars of the glycolipids of the whole cells and of the plasma membranes. Among sterols, the non-saponifiable fraction of the total lipids extracted from the trophozoites of pathogenic *Acanthamoeba* possesses ergosterol and 7-dehydrostigmasterol.⁴⁷ Therefore, lipids represent an essential source of energy storage, and can be expected to be targeted by *Acanthamoeba* during engagement with host cells for nutritional purposes and/or to modulate host-parasite interaction, including host inflammatory and immune responses.⁴⁹

Taken together, these findings indicate that although *A. castellanii* trophozoites can exist in a free-living status, their interaction with host cells involves changes in their metabolic and nutritional needs. With further improvements in the capabilities and sensitivity of RMS, it might be possible in the future to study the molecular trafficking and turnover of multiple amino acids simultaneously, as well as isotope labelled lipids. Further research on the molecular basis of amino acid sensing in *A. castellanii* will benefit therapeutic development and ultimately enhance our success at combating this important pathogen.

Acknowledgements

This work was supported by Petplan Charitable Trust grant 11-38 (H. Elsheikha and I. Notingher). A. Naemat acknowledges the support from COMSATS Institute of Information Technology, Pakistan. The development of the Raman micro-spectrometer was supported by the Biotechnology and Biological Sciences Research Council UK research grant BB/G010285/1.

References

- [1] J. K. Stehr-Green, T. M. Bailey and G. S. Visvesvara, *Am. J. Ophthalmol.* **1989** ; 107, 331.
- [2] V. Muñoz and H. Reyes, *Santiago de Chile Parasitol. Latinoam.* **2003** ; 58, 106.
- [3] C. Paszko-Kolva and H. Yamamoto, *Appl. Env. Microbiol.* **1991** ; 57, 163.
- [4] K. F. Van and H. Alizadeh, *Invest. Ophthalmol. Vis. Sci.* **1993** ; 34, 1937.
- [5] R. J. Neff and R. H. Neff, *Symp. Soc. Exp. Biol.* **1969** ; 23, 51.
- [6] B. Bowers and E. D. Korn, *J. Cell Biol.* **1968** ; 39, 95.
- [7] B. Bowers and E. D. Korn, *J. Cell Biol.* **1969** ; 41, 786.
- [8] F. Marciano-Cabral and G. Cabral, *Clin. Microbiol. Rev.* **2003** ; 16, 273.
- [9] Di Cave, R. Monno, P. Bottalico, S. Guerriero, S. D'Amelio, C. D'Orazi, F. Berrilli, *Eur. J. Clin. Microbiol. Infect. Dis.* **2009** ; 28(6), 607.
- [10] C. T. Price, T. Al-Quadani, M. Santic, I. Rosenshine and Y. Abu Kwaik, *Science* **2011** ; 334, 1553.
- [11] C. T. Price, A. M. Richards, J. E. Von Dwingelo, H. A. Samara and Y. Abu Kwaik, *Environ. Microbiol.* **2014** ; 16, 350.
- [12] E. Schunder, N. Gillmaier, E. Kutzner, W. Eisenreich, V. Herrmann, M. Lautner and K. Heuner, *J. Biol Chem.* **2014** ; 289, 21040.
- [13] F. L. Henriquez, S. J. Campbell, B. K. Sundararaj, A. Cano A, S. P. Muench and C. W. Roberts, *Protist* **2015** ; 166, 93.
- [14] D. Shipp, F. Sinjab, and I. Notingher, *Adv. Opt. Photon.* **2017** 9; 315.
- [15] B. Kann, H. L. Offerhaus, M. Windbergs and C. Otto, *Adv. Drug Deliv. Rev.* **2015** ; 89, 71.

- 1
2
3 [16] M. Okada, N. I. Smith, A. F. Palonpon, H. Endo, S. Kawata, M. Sodeoka and K.
4
5 Fujita, *Proc. Natl. Acad. Sci. USA*. **2012** ; 109, 28.
6
7
8 [17] F. C. Pascut, S. Kalra, V. George, N. Welch, C. Denning and I. Notingher, *Biochim.*
9
10 *Biophys. Acta*. **2013** ; 1830, 3517.
11
12 [18] A. Ghita, F. C. Pascut, V. Sottile V and I. Notingher, *Analyst* **2014** ; 139, 55.
13
14 [19] B. R. Wood, S. J. Langford, B. M. Cooke, F. K. Glenister, J. Lim and
15
16 D. McNaughton, *FEBS Lett.* **2003** ; 554, 247.
17
18 [20] S. Bonifacio, S. Finaurini, C. Krafft, S. Parapini, D. Taramelli and V. Sergio, *Anal.*
19
20 *Bioanal. Chem.* **2008** ; 392, 1277.
21
22 [21] A. J. Hobro, A. Konishi, C. Coban and N. I. Smith, *Analyst* **2013** ; 138, 3927.
23
24 [22] K. Kong, C. J. Rowlands, H. Elsheikha and I. Notingher, *Analyst* **2012** ; 137, 4119.
25
26 [23] A. Naemat, H. M. Elsheikha, A. Al-Sandaqchi, K. Kong, A. Ghita and I. Notingher,
27
28 *Analyst* **2015** ; 140, 756.
29
30 [24] A. Naemat, H. M. Elsheikha, R. A. Boitor and I. Notingher, *Sci. Rep.* **2016** ; 6, 20811.
31
32 [25] S. Haider, M. Wagner, M. C. Schmid, B. S. Sixt, J. G. Christian, G. Häcker, P.
33
34 Pichler, K. Mechtler, A. Müller, C. Baranyi, E. R. Toenshoff, J. Montanaro and M. Horn,
35
36 *Mol. Microbiol.* **2010** ; 77, 687.
37
38 [26] W. E. Huang, K. Stoecker, R. Griffiths, L. Newbold, H. Daims, A. S. Whiteley and
39
40 M. Wagner, *Environ. Microbiol.* **2007** ; 9, 1878.
41
42 [27] C. Matthäus, A. Kale, T. Chernenko, V. Torchilin and M. Diem, *Mol. Pharm.* **2008** ;
43
44 5, 287.
45
46 [28] H. J. van Manen, A. Lenferink, and C. Otto, *Anal. Chem.* **2008** ; 80, 9576.
47
48 [29] C. Matthäus, C. Krafft, B. Dietzek, B. R. Brehm, S. Lorkowski and J. Popp, *Anal.*
49
50 *Chem.* **2012**, 84, 8549.
51
52 [30] H. N. Noothalapati Venkata and S. Shigeto, *Chem. Biol.* **2012** ; 19, 1373.
53
54
55
56
57
58
59
60

- 1
2
3 [31] Y. C. Lin, E. Perevedentseva and C. L. Cheng, *J. Biomed. Opt.* **2015** ; 20(5), 51042.
4
5 [32] G. Rusciano, P. Capriglione, G. Pesce, S. Del Prete S, G. Cennamo, D. Di Cave, L.
6
7 Cerulli and A. Sasso, *PLoS One* **2013** ; 8, e72127.
8
9 [33] A. Zumbusch, G.R. Holtom, and X.S. Xie, *Phys. Rev. Lett.* **1999** ; 82(20), 4142.
10
11 [34] C.L. Evans, and X.S. Xie, *Annu. Rev. Anal. Chem.* **2008** ; 1, 883.
12
13 [35] W. Min, C.W. Freudiger, S. Lu, and X.S. Xie, *Annu. Rev. Phys. Chem.* **2011** ; 62, 507.
14
15 [36] R. Mouras, P. O. Bagnaninchi, A. R. Downes and A. P. D. Elfick, *J. Biomed. Opt.*
16
17 **2012** ; 17, 116011.
18
19 [37] T. Hellerer, C. Axäng, C. Brackmann, P. Hillertz, M. Pilon M and A. Enejder, *Proc*
20
21 *Natl Acad Sci U.S.A.* **2007** ; 104, 14658.
22
23 [38] R. Mouras, P. Bagnaninchi, A. Downes, and A. Elfick, *J. Raman Spectrosc.* **2013** ;
24
25 44, 1373.
26
27 [39] F. De Chaumont, S. Dallongeville, N. Chenouard, N. Hervé, S. Pop, T. Provoost, V.
28
29 Meas-Yedid, P. Pankajakshan, T. Lecomte, Y. Le Montagner, T. and Lagache, *Nature*
30
31 *Methods* **2012** ; 9(7), 690.
32
33 [40] N. Siamwiza, R. C. Lord, M. C. Chen, T. Takamatsu, I. Harada, H. Matsuura and T.
34
35 Shimanouchi, *Biochemistry* **1975** ; 14, 4870.
36
37 [41] M. Hurt, S. Neelam, J. Niederkorn and H. Alizadeh, *Infect. Immun.* **2003** ; 71, 6243.
38
39 [42] D. R. Ledee, A. Iovieno, D. Miller, N. Mandal, M. Diaz, J. Fell, M. E. Fini and E. C.
40
41 Alfonso, *J. Clin. Microbiol.* **2009** ; 47, 1458.
42
43 [43] W. D. Dolphin, *J. Protozool.* **1976** ; 23, 455.
44
45 [44] O. P. Shukla, S. M. Kaul and R. K. Mehlotra, *J. Protozool.* **1990** ; 37, 237–242.
46
47 [45] M. Clarke, A. J. Lohan, B. Liu, I. Lagkouvardos, S. Roy, N. Zafar, C. Bertelli, C.
48
49 Schilde, A. Kianianmomeni, T. R. Bürglin, C. Frech, B. Turcotte, K. O. Kopec, J. M.
50
51 Synnott, C. Choo, I. Paponov, A. Finkler, C. S. Heng Tan, A. P. Hutchins, T. Weinmeier,
52
53
54
55
56
57
58
59
60

1
2
3 T. Rattei, J. S. Chu, G. Gimenez, M. Irimia, D. J. Rigden, D. A. Fitzpatrick, J. Lorenzo-
4 Morales, A. Bateman, C. H. Chiu, P. Tang, P. Hegemann, H. Fromm, D. Raoult, G.
5 Greub, D. Miranda-Saavedra, N. Chen, P. Nash, M. L. Ginger, M. Horn, P. Schaap, L.
6 Caler and B. J. Loftus, *Genome Biol.* **2013** ; 14, R11.

7
8
9
10
11
12 [46] D. G. Dearborn and E. D. Korn, *J Biol Chem.* **1974** ; 249, 3342.

13
14 [47] F. R. Smith and E. D. Korn, *J Lipid Res.* **1968** ; 9, 405.

15
16 [48] A. G. Ulsamer, P. L. Wright, M. G. Wetzel and E. D. Korn, *J Cell Biol.* **1971** ; 51,
17
18 193.

19
20 [49] H. A. Saka and R. Valdivia, *Annu Rev Cell Dev Biol.* **2012** ; 28, 411.

21 22 23 24 25 26 27 **Figure Captions**

28
29
30 **Fig. 1** Raman spectroscopy measurements of typical *A. castellanii* trophozoites after 24 hours
31 of incubation in L-Phe(D8)-supplemented DMEM medium. (a) Brightfield image, (b)
32 Spectral maps of selected Raman bands and (c) Selected Raman spectra at the indicated
33 locations (i, ii, iii, iv) in the cell. Scale bar: 10 μm .

34
35
36
37
38
39
40
41
42
43 **Fig. 2** Raman spectral imaging of *A. castellanii* at 24 hours of incubation in L-Phe(D8)-
44 supplemented media. (a) Bright field, (b) Maps corresponding to Raman spectral peaks 1449
45 cm^{-1} , 1004 cm^{-1} , 960 cm^{-1} and (c) Average Raman spectra of *A. castellanii* trophozoites.
46
47
48
49 Scale bars: 10 μm .

1
2
3 **Fig. 3** The uptake of L-Phe(D8) by *A. castellanii* from ARPE-19 cells (a) Bright field image
4 and Raman spectral maps of ARPE-19 cells infected with *A. castellanii* at 24 hpi and (b)
5 Selected Raman spectra at the indicated locations. Scale bar: 10 μm .
6
7
8

9
10
11 **Fig. 4** Raman spectral imaging of ARPE-19 cells infected with *A. castellanii* at 24 hpi. (a)
12 Brightfield images and fluorescence images (recorded immediately after Raman spectroscopy
13 measurements), (b) Maps corresponding to Raman spectral peaks 1004 cm^{-1} and 960 cm^{-1} and
14 (c) Average Raman spectra of *A. castellanii* trophozoites and ARPE-19 cells. Scale bars: 10
15 μm .
16
17
18
19
20
21
22

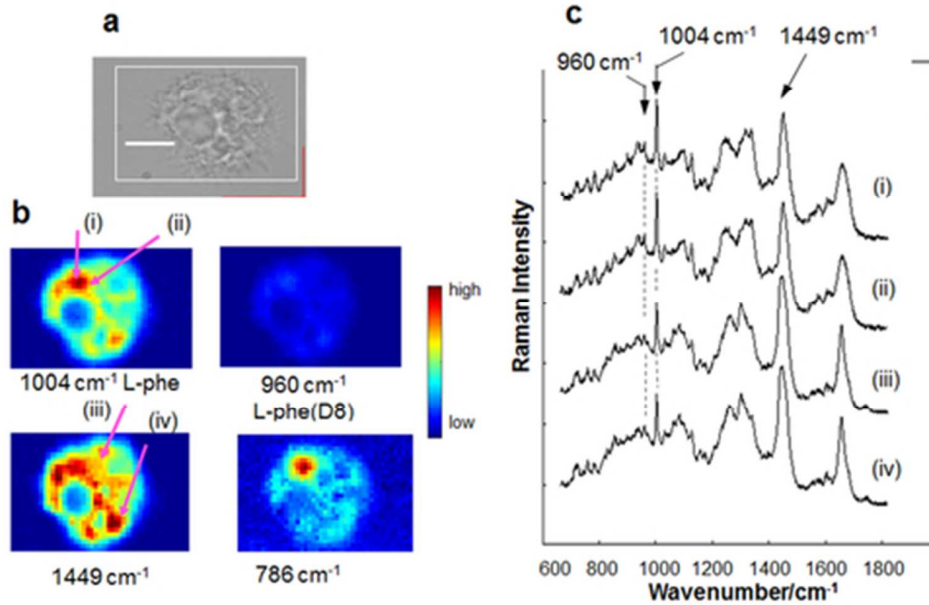
23
24
25 **Fig. 5** Raman spectral imaging of ARPE-19 cells infected with *A. castellanii* at 48 hpi.
26 Raman spectral images and selected Raman spectra of ARPE-19 cells infected with *A.*
27 *castellanii* at 48 hpi. Scale bar: 10 μm
28
29
30
31

32
33
34 **Fig. 6** Raman spectral imaging of ARPE-19 cells infected with *A. castellanii* at 48 hpi. (a)
35 Bright field images and fluorescence images (recorded immediately after Raman
36 spectroscopy measurements), (b) Maps corresponding to Raman spectral peaks 1004 cm^{-1} and
37 960 cm^{-1} and (c) Average Raman spectra from *A. castellanii* trophozoites and ARPE-19 cells.
38
39
40
41
42
43
44
45
46
47
48
49
50
51
52
53
54
55
56
57
58
59
60

59
60 **Fig. 7** Kinetics of the uptake of L-Phe(D8) by *A. castellanii* from host cells. (a) Uptake of L-
Phe(D8) by *A. castellanii* from ARPE-19 cells: calculated ratio $I_{960}/(I_{1004}+I_{960})$ ($n=6$ cells at
each time point). (b) Computed difference Raman spectra for *A. castellanii* infecting ARPE-
19 cells at 24 and 48 hpi and *A. castellanii* cells in L-Phe(D) media at 24 hours. Spectra are
shifted vertically for clarity.

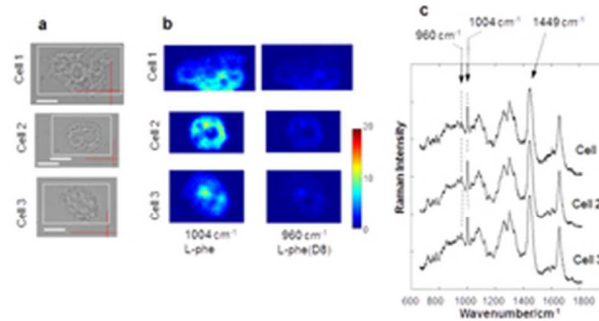
1
2
3 **Fig 8.** CARS microscopy of fixed *A. castellani* and ARPE-19 cells at (a) 3h, (b) 24h and (c)
4 48h post-infection. (d) Control cells represent cell-free parasites identified at 3hrs. Image
5 contrast is generated from the C-H₂ symmetric stretching band at 2845cm⁻¹, which is
6 primarily from lipid structures. The images provide complementary high-resolution three-
7 dimensional structural information generated primarily from endogenous lipid structures,
8 allowing the interface between *A. castellani* and ARPE-19 cells to visualized. Lipid droplet
9 structures near the interface at 48 hours.
10
11
12
13
14
15
16
17
18
19
20
21
22
23
24
25
26
27
28
29
30
31
32
33
34
35
36
37
38
39
40
41
42
43
44
45
46
47
48
49
50
51
52
53
54
55
56
57
58
59
60

For Peer Review



Raman spectroscopy measurements of typical *A. castellanii* trophozoites after 24 hours of incubation in L-Phe(D8)-supplemented DMEM medium. (a) Brightfield image, (b) Spectral maps of selected Raman bands and (c) Selected Raman spectra at the indicated locations (i, ii, iii, iv) in the cell. Scale bar: 10 μm .

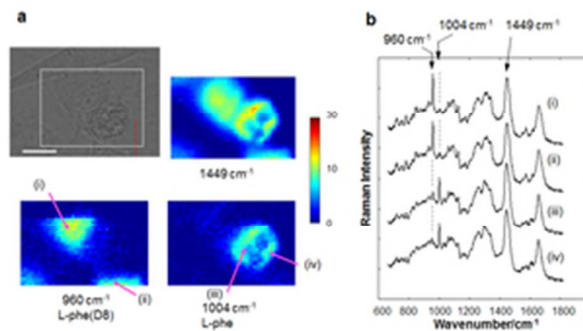
41x27mm (300 x 300 DPI)



Raman spectral imaging of *A. castellanii* at 24 hours of incubation in L-Phe(D8)-supplemented media. (a) Bright field, (b) Maps corresponding to Raman spectral peaks 1449 cm⁻¹, 1004 cm⁻¹, 960 cm⁻¹ and (c) Average Raman spectra of *A. castellanii* trophozoites. Scale bars: 10 μ m.

27x14mm (300 x 300 DPI)

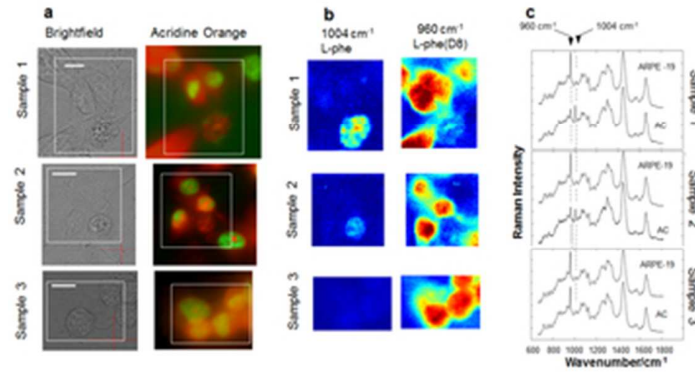
Peer Review



The uptake of L-Phe(D8) by *A. castellanii* from ARPE-19 cells (a) Bright field image and Raman spectral maps of ARPE-19 cells infected with *A. castellanii* at 24 hpi and (b) Selected Raman spectra at the indicated locations. Scale bar: 10 μm .!! †

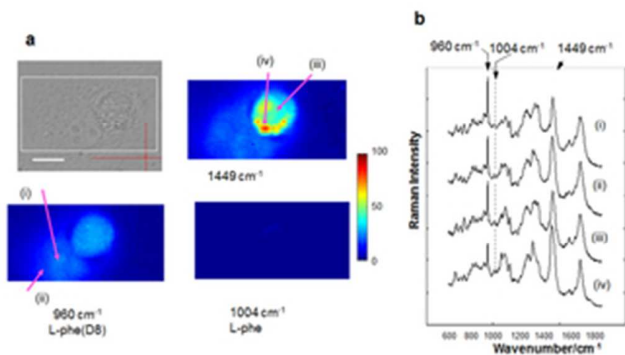
26x14mm (300 x 300 DPI)

Peer Review



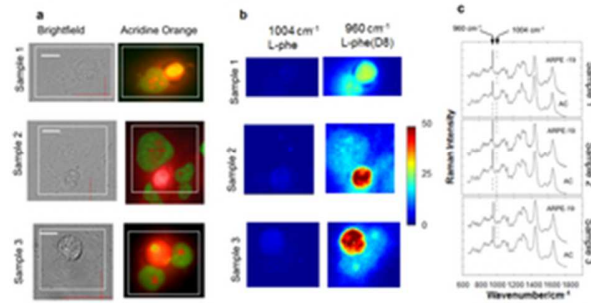
Raman spectral imaging of ARPE-19 cells infected with *A. castellanii* at 24 hpi. (a) Brightfield images and fluorescence images (recorded immediately after Raman spectroscopy measurements), (b) Maps corresponding to Raman spectral peaks 1004 cm⁻¹ and 960 cm⁻¹ and (c) Average Raman spectra of *A. castellanii* trophozoites and ARPE-19 cells. Scale bars: 10 μ m.

30x16mm (300 x 300 DPI)

1
2
3
4
5
6
7
8
9
10
11
12
13
14
15
16
17
18
19
20
21
22
23
24
25
26
27
28
29
30
31
32
33
34
35
36
37
38
39
40
41
42
43
44
45
46
47
48
49
50
51
52
53
54
55
56
57
58
59
60

Raman spectral imaging of ARPE-19 cells infected with *A. castellanii* at 48 hpi. Raman spectral images and selected Raman spectra of ARPE-19 cells infected with *A. castellanii* at 48 hpi. Scale bar: 10 μ m

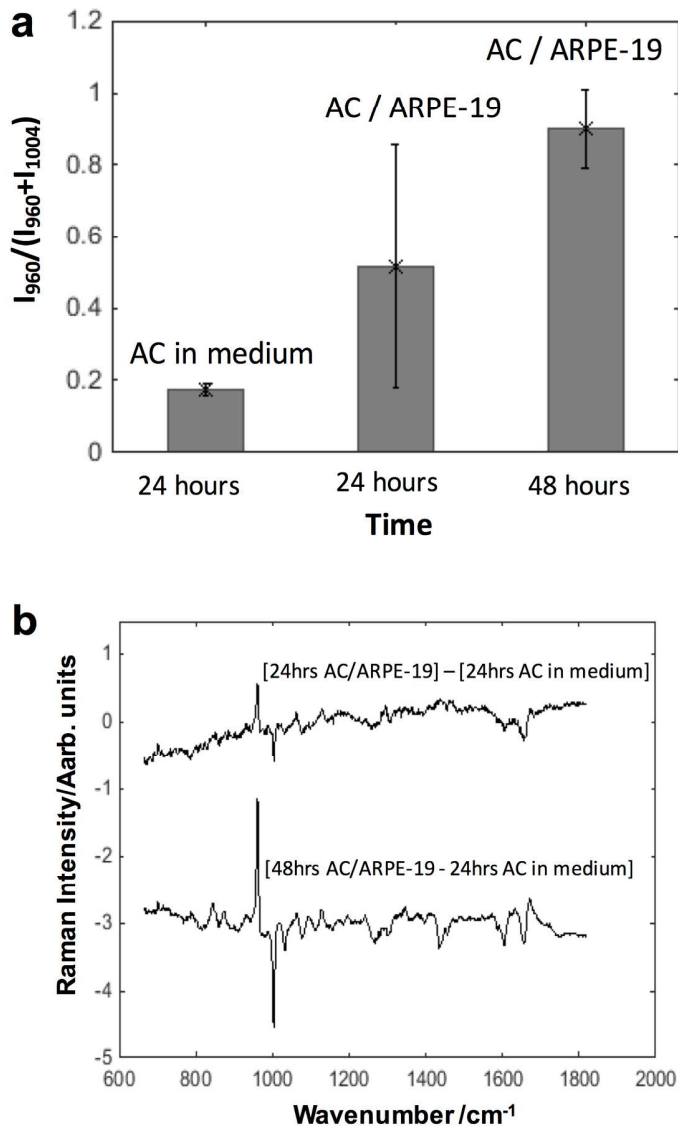
27x15mm (300 x 300 DPI)



Raman spectral imaging of ARPE-19 cells infected with *A. castellanii* at 48 hpi. (a) Bright field images and fluorescence images (recorded immediately after Raman spectroscopy measurements), (b) Maps corresponding to Raman spectral peaks 1004 cm⁻¹ and 960 cm⁻¹ and (c) Average Raman spectra from *A. castellanii* trophozoites and ARPE-19 cells. Scale bars: 10 μ m.

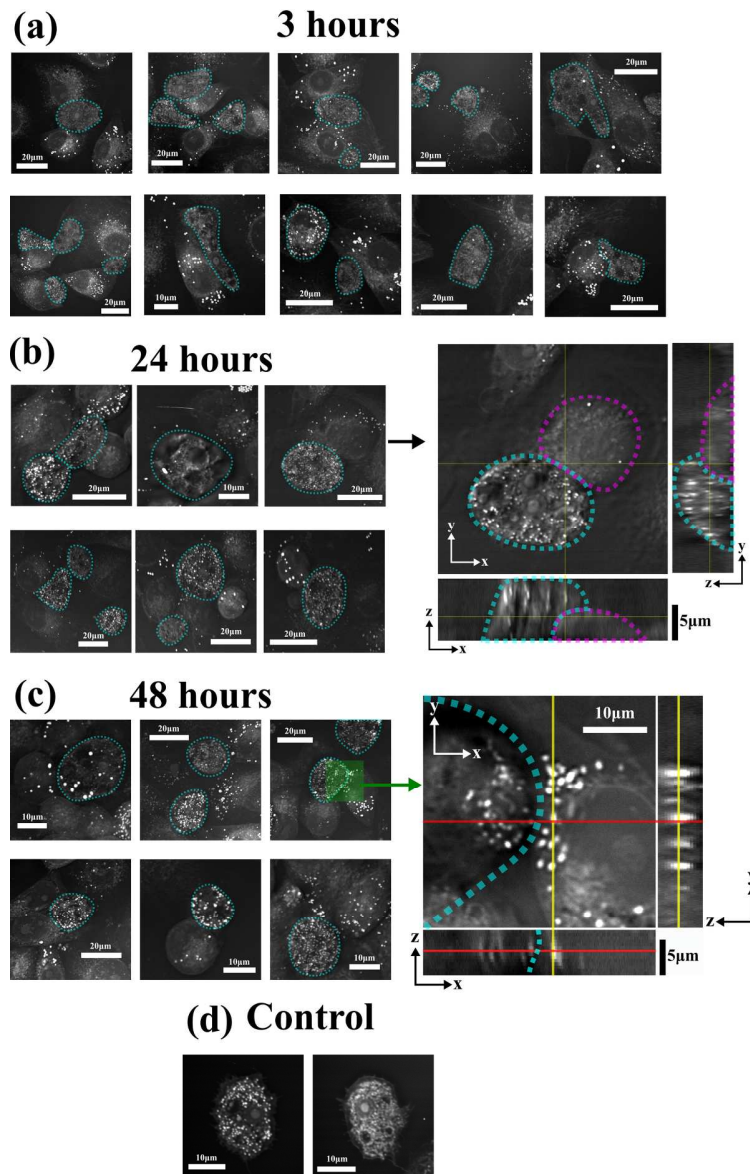
25x13mm (300 x 300 DPI)

Peer Review



Kinetics of the uptake of L-Phe(D8) by *A. castellanii* from host cells. (a) Uptake of L-Phe(D8) by *A. castellanii* from ARPE-19 cells: calculated ratio $I_{960}/(I_{1004}+I_{960})$ ($n=6$ cells at each time point). (b) Computed difference Raman spectra for *A. castellanii* infecting ARPE-19 cells at 24 and 48 hpi and *A. castellanii* cells in L-Phe(D) media at 24 hours. Spectra are shifted vertically for clarity.

148x226mm (300 x 300 DPI)



CARS microscopy of *A. castellanii* and ARPE-19 cells at (a) 3h, (b) 24h and (c) 48h post-infection. (d) Control cells represent cell-free parasites identified at 3hrs. Image contrast is generated from the C-H2 symmetric stretching band at 2845cm^{-1} , which is primarily from lipid structures. The images provide complementary high-resolution three-dimensional structural information generated primarily from endogenous lipid structures, allowing the interface between *A. castellanii* and ARPE-19 cells to be visualized. Lipid droplet structures near the interface at 48 hours.

152x237mm (300 x 300 DPI)

